Solid lipid Nanocarriers diffuse effectively through mucus and enter intestinal cells – *but where is my peptide?*

Camille Dumont [a,b], Ana Beloqui [c], Cédric Miolane [a], Sandrine Bourgeois [b,d], Véronique Préat [c], Hatem Fessi [b, d], Vincent Jannin [a, †]

[a] Gattefossé SAS, 36 chemin de Genas 69804 Saint-Priest cedex, France

[b] Univ Lyon, Université Claude Bernard Lyon 1, CNRS, LAGEPP UMR 5007, 43 boulevard du 11 novembre 1918, F-69100, VILLEURBANNE, France

[c] Université catholique de Louvain, Louvain Drug Research Institute, Advanced Drug Delivery and Biomaterials, 1200 Brussels, Belgium.

[d] Univ Lyon, Université Claude Bernard Lyon 1, ISPB-Faculté de Pharmacie de Lyon, F-69008, Lyon, France

Corresponding author :

Dr. HDR Vincent Jannin

Lonza Pharma & Biotech, Parc d'Innovation, Rue Tobias Stimmer – BP 30442 – 67412 Illkirch Graffenstaden, France

Phone: +33 3 89 20 49 71

vincent.jannin@lonza.com

[†] Current address: Lonza Pharma & Biotech, Parc d'Innovation, Rue Tobias Stimmer – BP 30442 – 67412 Illkirch Graffenstaden, France

1. Abstract

Peptides are therapeutic molecules with high potential to treat a wide variety of diseases. They are large hydrophilic compounds for which absorption is limited by the intestinal epithelial border covered by mucus. This study aimed to evaluate the potential of Hydrophobic Ion Pairing combined with Solid Lipid Nanoparticles (SLN) and Nanostructured Lipid Carriers (NLC) to improve peptide transport across the intestinal border using Caco-2 cell monolayers (enterocyte-like model) and Caco-2/HT29-MTX co-cultured monolayers (mucin-secreting model). A Hydrophobic Ion Pair (HIP) was formed between Leuprolide (LEU), a model peptide, and sodium docusate. The marked increase in peptide lipophilicity enabled high encapsulation efficiencies in both NLC (84%) and SLN (85%). After co-incubation with the nanoparticles, confocal microscopy images of the cell monolayers demonstrated particles internalization and ability to cross mucus. Flow cytometry measurements confirmed that 82% of incubated SLN and 99% of NLC were internalized by Caco-2 cells. However, LEU transport across cell monolayers was not improved by the nanocarriers. Indeed, combination of particles platelet-shape and HIP low stability in the transport medium led to LEU burst release in this environment. Improvement of peptide lipidization should maintain encapsulation and enable benefit from nanocarriers enhanced intestinal transport.

Keywords: peptide, intestinal permeability, Hydrophobic Ion Pair, Solid Lipid Nanoparticles, Nanostructured Lipid Carriers, cell models

Highlights:

- Formation of HIP enables high encapsulation efficiency of peptide in SLN and NLC
- Lipid-based nanocarriers were highly internalized by Caco-2 cell monolayers
- SLN and NLC were able to cross the mucus barrier (Caco-2/HT29-MTX cell model)
- Peptide intestinal transport was limited by an extensive release from the carriers

54 Abbreviations:

55 CLSM: Confocal Laser Scanning Microscope, C90: Capryol®90, DiD: 1,1'-Dioctadecyl-3,3,3',3'-
56 Tetramethylindodicarbocyanine, 4-Chlorobenzenesulfonate Salt, DMEM: Dulbecco's Modified Eagle
57 Medium, ELISA: Enzyme-linked immunosorbent assay, FaSSIF: Fasted State Simulated Intestinal Fluid,
58 FBS: Fetal Bovine Serum, HBSS: Hank's Balanced Salt Solution, HIP: Hydrophobic Ion Pair, HPH: High
59 Pressure Homogenization, HPLC: High Pressure Liquid Chromatography, LEU: Leuprolide, MEM NEAA
60 : Minimum Essential Medium Non-Essential Amino Acids, MTT: 3-(4,5-dimethylthiazol-2-yl)-2,5-
61 diphenyltetrazolium, NLC: Nanostructured Lipid Carrier, P_{app}: apparent permeability, PATO5:
62 Precirol® ATO 5, RH40: Kolliphor® RH40, SEDDS: Self-Emulsifying Drug Delivery System, SLN: Solid
63 lipid Nanoparticle, TEER: Transepithelial Electric Resistance, TFA: Trifluoroacetic acid

64

65 ## 2. Introduction

66 Interest in the use of peptides as therapeutic molecules has been growing over the last
67 decades. This is particularly due to their specific binding capacity with the *in vivo* target,
68 enabling high potency with few adverse effects. Currently, most of these molecules are
69 parenterally administered to reach acceptable levels of efficacy. Although oral
70 administration would result in higher patient compliance and reduced industrial costs,
71 peptides exhibit poor oral bioavailability (generally inferior to 1%) (Brayden and O'Mahony,
72 1998). Indeed, upon oral administration, peptides encounter a succession of barriers limiting
73 their possibility to reach the systemic circulation. The fist barrier is a chemical barrier:
74 peptides undergo enzymatic degradation initiated by proteases which degrade
75 macromolecules into absorbable nutrients. The second barrier corresponds to the mucus
76 layer. Mucus is produced by goblet cells and is about 100 to 200 µm thick in human adults.
77 This negatively charged gel layer can interact with biomolecules, blocking them at its
78 surface, and prevent their passage (Leonaviciute and Bernkop-Schnürch, 2015). The third
79 barrier, the epithelial layer, is mainly composed of enterocytes (~99%), separated by tight
80 junctions. The passage of peptides across this cell layer is hindered for two reasons: their
81 hydrophilic character prevents their transcellular permeation across the lipophilic plasma
82 membrane of the cells, and their size limits the paracellular pathway through tight junctions
83 whose diameter is evaluated at 0.52 nm in human duodenum (Li et al., 2012).

84 Lipid-based carriers, composed of biocompatible and biodegradable excipients seem a
85 promising and safe answer to address peptides oral limitations (Almeida et al., 1997;
86 Dumont et al., 2018; Geszke-Moritz and Moritz, 2016; Li et al., 2012, Xu et al., 2019).
87 However, alteration of their hydrophilic character is required to reach interesting payloads in
88 these formulations. The formation of Hydrophobic Ion Pairs (HIP) has been widely reported
89 for this purpose as it enables a reversible increase in lipophilicity without altering the
90 structure of the therapeutic drug (Phan et al., 2019; Ristroph and Prud'homme, 2019). The
91 encapsulation of a peptide lipidized as HIP in Self-Emulsifying Drug Delivery Systems (SEDDS)
92 has provided a protective effect towards enzymatic degradation (Hetényi et al., 2017), has
93 enabled an increased mucus permeation (Griesser et al., 2018) and has allowed increasing
94 oral bioavailability up to 17.2-fold in rats (Hintzen et al., 2014) and 17.9-fold in pigs
95 (Bonengel et al., 2018).

96 Regarding solid lipid nanocarriers, Shrestha *et al.* encapsulated two large peptides, exenatide
97 (logP=-2.1) and liraglutide (logP=-3.4) in Nanostructured Lipid Carriers (NLC) (Shrestha et al.,
98 2018). However, increase in peptide across Caco-2 cell monolayers was only observed for
99 exenatide. .

100 Our group has already demonstrated the possibility to increase the Entrapment Efficiency
101 (EE) and drug loading of a peptide in NLC and Solid Lipid Nanocarriers (SLN) after formation
102 of a HIP (Dumont et al., 2019a). The nanosuspensions were obtained by hot High Pressure
103 Homogenization (HPH), a scalable and solvent-free technique (Dumont et al., 2018). The
104 nanoparticles were neutral, platelet-shaped, measured around 100 nm and have shown a
105 protective effect towards trypsin-induced degradation. Although the platelet shape of the
106 particles is a disadvantage regarding the drug release in Fasted Simulated Intestinal Fluid
107 (FaSSIF-V2) containing phospholipids, this structure should be an advantage to increase their
108 passage across the intestinal epithelium. Indeed, in the case of polymeric nanoparticles,
109 absorption was higher for platelet-shaped nanoparticles compared to spherical ones
110 (Banerjee et al., 2016; Doshi Nishit and Mitragotri Samir, 2010). Then, this study aims to
111 evaluate if the peptide remaining encapsulated in the solid lipid nanocarriers can be
112 transported across mucus and epithelial cells to finally increase peptide absorption.

113 Intestinal cell models were used to evaluate the intestinal passage of the formulations. Caco-
114 2 cells are widely used as enterocyte-like model in *in vitro* intestinal permeability. Originally
115 obtained from human epithelial colorectal adenocarcinoma cells, these cells are widely used
116 as they spontaneously differentiate in human enterocytes, exhibiting tight junctions,
117 microvilli on the apical surface and small intestine hydrolase activities (Sambuy et al., 2005).
118 Mucin-secreting intestinal cell models were developed to better mimic the intestinal border,
119 using co-cultures of Caco-2 and HT29-MTX (goblet cells) (Béduneau et al., 2014; Chen et al.,
120 2010; Lesuffleur et al., 1993). The mucus layer present at the apical side of the coculture
121 allows a more biorelevant use of the cell-based membrane. Indeed, this coculture can be
122 used with biorelevant media, pancreatic enzymes (Antoine et al., 2015) and lipid-based
123 excipients exhibiting surfactant properties (Dubray et al., 2016).

124 In the present study, Leuprolide, a hydrophilic peptide model, was encapsulated by HPH in
125 NLC and SLN after formation of a HIP with sodium docusate. This anionic surfactant enables

126 marked increase in log P, high precipitation efficiency and can favor the passage of
127 molecules by fluidization of the enterocytes membranes (Anderberg et al., 1992; Griesser et
128 al., 2017). The HIP-loaded nanoparticles were characterized regarding their size,
129 polydispersity index (PDI), EE and drug loading (D_L). The ability of these lipid
130 nanosuspensions to transport Leuprolide across the mucus layer and cell-based membrane
131 was evaluated using either Caco-2 cell monolayers or the Caco-2/HT29-MTX mucin-secreting
132 model. The transport capacity of NLC and SLN was compared as well as their internalization
133 by the cells.

134

135 # 3. Material and methods

136 ## 3.1. Materials

137 Leuprolide acetate was obtained from Glentham Life Sciences (LEU, Corsham, UK). Sodium
138 docusate, used for the preparation of the HIP, was purchased from Sigma Aldrich.

139 Nanoparticles were formulated with Precirol® ATO 5 (glyceryl distearate, PATO5,
140 Gattefossé), Capryol® 90 (propylene glycol monocaprylate, C90, Gattefossé) and Kolliphor®
141 RH40 (PEG-40 hydrogenated castor oil, RH40, Sigma Aldrich).

142 1,1'-Dioctadecyl-3,3,3',3'-Tetramethylindodicarbocyanine, 4-Chlorobenzenesulfonate Salt
143 (DiD, Invitrogen) and rhodamine-phalloidin (Invitrogen) were purchased from Thermofisher.
144 Vectashield mounting medium was obtained from Labconsult. Alcian Blue 8GX, Thizoyl Blue
145 Tetrazolium Bromide and Triton X-100 were obtained from Sigma Aldrich. Matrigel™ was
146 purchased to BD Bioscience.

147 The Caco-2 cell line was kindly provided by Dr Maria Rescigno (University of Milano-Bicocca,
148 Milano, Italy) and used from passages X+25 to 30. The HT29-MTX cell lines were kindly
149 donated by Dr. Arnaud Beduneau from Université de Franche-Comté, Besançon, France, and
150 used between passages X+50 to 62. Dulbecco's Modified Eagle Medium (DMEM, ref 41965-
151 039), Dulbecco's Phosphate Buffered Saline (DPBS, ref 14190-094), Hank's Balanced Salt
152 Solution (HBSS, ref 14175-053), Minimum Essential Medium Non-Essential Amino Acids
153 (MEM NEAA), L-glutamine and Penicillin-Streptomycin were purchased from Gibco. Fetal
154 Bovine Serum (FBS) HyClone™ were purchased from GE Healthcare. Leuprolide ELISA kit (S-

155 1144) was obtained from BMA Biomedicals. Trifluoroacetic acid (TFA) was obtained from
156 Sigma Aldrich. Tetrahydrofuran (THF) and Acetonitrile used were in the HPLC grade.

157

158 ## 3.2. Methods

159 ### 3.2.1. HPLC analysis

160 LEU was quantified using an Alliance 2695D (Waters, Saint-Quentin-en-Yvelines, France)
161 equipped with a UV detector (2487, Waters). Separation was achieved using a Kinetex EVO
162 C18 100 Å 2.6 µm 50x4.6 mm column (Phenomenex, Le Pecq, France) at 40°C. A linear
163 gradient of elution was applied from 15% solvent A/85% solvent B to 50% solvent A/50%
164 solvent B (solvent A: water with 0.1% (v/v) TFA; solvent B: acetonitrile). The flow rate was
165 set at 0.7 mL/min, the injection volume was 20 µL and the wavelength of the detector was
166 set at 217 nm. The calibration curve was established between 10 and 100 µg/mL and the
167 Lower Limit of Quantification (LLOQ) was found to be 1 µg/mL.

168

169 ### 3.2.2. Formation of HIP

170 The method used for the formation of the leuprolide-docusate HIP (molar ratio 1:2
171 LEU:docusate) has been previously described (Dumont et al., 2019). Briefly, 20 mg of LEU
172 were ionized in 1 mL of 0.01 M HCl. Then, 1 mL of a 14 mg/mL sodium docusate solution was
173 added to LEU solutions. The immediate formation of a white precipitate confirmed the
174 formation of the ion pair. The complexes were centrifuged for 10 minutes at 15000 g, 4°C
175 using a Universal Centrifuge 320 R (Hettich). The supernatants were collected and analyzed
176 *via* HPLC (see 2.2.1.) to quantify the amount of LEU remaining free. The results were used to
177 calculate the precipitation efficiency, Equation 1.

178 The HIP were frozen in liquid nitrogen, lyophilized and stored at -20°C until further use.

179

180 *Equation 1: Calculation of precipitation efficiency of HIP formation*

$$Precipitation\ efficiency, \% = 100 - (100\ X\ \frac{[LEU]_{supernatant}}{[LEU]_{initial}})$$

181

182 3.2.3. NLC and SLN formulation

183 A HPH technique was used to prepare both type of nanoparticles, as previously described by
184 (Dumont et al., 2019a). The composition of the nanoparticles was adapted from previous
185 studies and is detailed in Table 1 (Dumont et al., 2019a, 2019b). PATO5 and DiD (when
186 specified), were melted under magnetic stirring at 70°C in a water bath. The HIP was added
187 to the melted lipid phase either as a solid, for SLN formulations, or dissolved in C90 for NLC
188 formulations. The lipid phase was let to homogenize under 400 rpm magnetic stirring for 10
189 min. The aqueous phase containing RH40, also heated at 70°C, was added to the mixture and
190 homogenized for 3 min at 11 000 rpm (Ultra-Turrax® T18, IKA). Next, the formed O/W
191 emulsion was introduced in the high-pressure homogenizer (Microfluidizer®LM20,
192 Microfluidics) and subjected to 5 cycles at 500 bar. The resulting nanoemulsion was then
193 collected and placed for 10 minutes at 4°C in an ice/water bath under 400 rpm to form the
194 solid nanoparticles. The nanosuspensions were stored at 4°C.

195 *Table 1: Nanoparticles composition*

	NLC-HIP	NLC-HIP-DiD	SLN-HIP	SLN-HIP-DiD
PATO5	4.00 g	4.00 g	4.00 g	4.00 g
C90	300 µL	300 µL	-	-
RH40	1.60 g	1.60 g	1.60 g	1.60 g
HIP (LEU)	29 mg (16 mg)	29 mg (16 mg)	29 mg (16 mg)	29 mg (16 mg)
DiD	-	1 mg	-	1 mg

196

197 ## 3.3. Nanoparticles characterization

198 3.3.1. Particle size distribution

199 The particle size distribution and PDI of the nanoparticles were measured *via* Dynamic Light
200 Scattering (DLS) using a Zetasizer Nano ZS (Malvern) at 25°C on samples diluted in water,
201 one droplet in 2 mL (dynamic viscosity: 8.90×10^{-4} Pa.s). Results are expressed as mean Z-
202 average ± standard error of mean (SEM).

203

204 3.3.2. Encapsulation efficiency and drug loading

205 The EE and D_L are defined in Equation 2 and Equation 3, respectively. To determine the total
206 amount of drug, 500 µL of nanoparticles were dissolved in 500 µL of THF to dissolve PATO5.
207 Then, 500 µL of this solution were mixed with 500 µL MeOH + 0.1% TFA. This solution was

208 filtered (0.45 µm pore size) before analysis by HPLC (see 2.2.1). To quantify the
209 unencapsulated amount of LEU, the suspensions were diluted in MilliQ water and filtered
210 upon centrifugation at 12 000 g for 15 min at 4°C using Eppendorfs equipped with 0.1 µm
211 PVDF filters (Ultrafree®-MC VV, Merck Millipore).

212 *Equation 2: Encapsulation efficiency calculation*

$$Encapsulation\ efficiency, \% = 100\ X\ \frac{Total\ amount\ of\ drug - unencapsulated\ amount\ of\ drug}{Total\ amount\ of\ drug}$$

213 *Equation 3: Drug loading calculation*

$$Drug\ loading, \mu g/mg = \frac{Total\ amount\ of\ drug - unencapsualted\ amount\ of\ drug}{Solid\ content}$$

214

215 ## 3.4. Cell culture studies

216 ### 3.4.1. Culture medium

217 Caco-2 and HT29-MTX cell lines were cultured in DMEM medium supplemented with 10%
218 FBS HyClone™, 1% Non-Essential Amino Acids, 1% L-Glutamine and 1%
219 Penicillin/Streptomycin. Cells were grown in incubator at 37°C with 10% CO_2. Medium was
220 changed every other day.

221

222 ### 3.4.2. Cytotoxicity evaluation

223 The impact of the nanosuspensions on Caco-2 and Caco-2/HT29-MTX cells viability was
224 evaluated with a 3-(4,5-dimethylthiazol-2-yl)-2,5-diphenyltetrazolium (MTT) colorimetric
225 assay. To that end, 96 well plates were first coated with Matrigel™ (10 µL/mL of DMEM) to
226 ensure a proper adhesion of the cells and emulate the conditions of the inserts. The wells
227 were rinsed twice with DMEM before seeding $2x10^4$ cells per well of Caco-2 or Caco-2:HT29-
228 MTX (ratio 3:1). Cells were allowed to grow overnight at 37°C, 10% CO_2. They were then
229 washed twice with pre-warmed HBSS at 37°C. 100 µL of nanosuspensions diluted in HBSS
230 were added in each well to reach final concentrations between 0.5 and 18 mg/mL of blank
231 particles. The same particle concentrations were used in the case of NLC-HIP and SLN-HIP
232 (corresponding to a total LEU concentration between 0.8 and 60 µg/mL). The negative
233 control corresponded to 4 wells containing only HBSS and the positive control corresponded

234 to 4 wells containing a 0.5% Triton solution. The formulations were incubated with the cells
235 during 2 h at 37°C. The wells were then washed twice with HBSS and 100 µL MTT solution in
236 DMEM (0.5 mg/mL) were added in each well. The plates were incubated for 3 h at 37°C. The
237 formazan purple crystals formed by the reaction of MTT with NAD(P)H of alive cells were
238 dissolved in 200 µL DMSO and the absorbance was measured at 450 nm on a Multiskan EX
239 plate reader (Thermo Fisher Scientific, MA, USA). The IC_{50} were calculated using GraphPad
240 Prism 8 program (CA, USA).

241

242 3.4.3. Transport study

243 The transport of LEU encapsulated in NLC and SLN was evaluated on both Caco-2 and Caco-
244 2:HT29-MTX (3:1) cell monolayers. To this end, PET cell culture inserts with a 1.0 µm pore
245 size (ref 353103, Falcon) were coated with 200 µL of a Matrigel™ solution (10 µL/mL in
246 DMEM). They were rinsed 3 times with DMEM before seeding $5x10^5$ Caco-2 cells or Caco-
247 2:HT29-MTX (3:1) cells in 500 µL culture medium. The cells were cultured for 21 days with
248 medium replacement every other day. On day 21, the inserts were washed 3 times with pre-
249 warmed HBSS at 37°C and allowed to equilibrate during 30 min in the incubator. Then, the
250 integrity of the cell monolayer was evaluated my measuring the TransEpithelial Electric
251 Resistance (TEER) with an epithelial voltohmmeter (EVOM², World Precision Instrument,
252 Berlin). The transport experiment was conducted only on inserts with TEER values over 200
253 Ω.cm².

254 The transport of LEU and LEU encapsulated in NLC and SLN across Caco-2 and Caco-2/HT29-
255 MTX cell monolayers was evaluated by addition of 500 µL LEU in HBSS, NLC-HIP-DiD diluted
256 in HBSS and SLN-HIP-DiD diluted in HBSS on the apical compartment. A concentration
257 equivalent to the IC_{50} (11 µg/mL of LEU) was used, considering that the number of cells used
258 for the transport study is much higher than for cytotoxicity measurements. The basolateral
259 chamber was filled with 1000 µL HBSS. The cells were incubated with the solutions during 2
260 h at 37°C. HBSS on the apical side was collected to quantify transported LEU by ELISA. The
261 results enabled the calculation of the apparent permeability (Papp, cm s^{-1}) as described in
262 Equation 4, where dQ/dt is the transport rate (µg/s), A is the surface area of the insert (cm²)
263 and C_0 is the initial concentration at the apical side (µg/mL).

264 *Equation 4: Apparent permeability calculation*

$$Papp = \frac{dQ}{dt} X \frac{1}{AC_0}$$

265 After 2h, the inserts were rinsed with cold HBSS to stop the transport and the cell
266 monolayers were fixed with a 4% paraformaldehyde solution for further observation by
267 Confocal Scanning Laser Microscope (CLSM), see 2.4.4.

268 To demonstrate the presence of mucus on the co-culture monolayers, some inserts were
269 plunged in Methacarn (60% methanol, 30% chloroform, 10% acetic acid) for 30 min at 4°C to
270 fix the cells. They were gently rinsed in DPBS before the addition of 200 µL of a 1% Alcian
271 blue solution in acidic medium (3% acetic acid, pH 2.5). After 45 min at room temperature,
272 the inserts were washed, cut and observed under the microscope (Axioskop 40, Carl Zeiss
273 Microscopy, USA). Images were taken with the Zen lite 2012 software.

274

275 3.4.4. Nanoparticle interaction with cell cultures

276 The interaction of the nanoparticles with Caco-2 cell and Caco-2/HT29-MTX cocultures was
277 evaluated both qualitatively and quantitatively.

278 The interaction of the nanoparticles and the cells was qualitatively evaluated using the
279 Zeiss™ confocal microscope (LSM 150, Zeiss, Germany) which enables to localize the NLC-
280 HIP-DiD and the SLN-HIP-DiD within the cell monolayers. The observation and images were
281 conducted on the inserts used for the transport study (2.4.3). Cell monolayers, fixed in
282 paraformaldehyde, were gently washed in DPBS. Actin was stained by adding of 200 µL of a
283 0.5% Triton solution in DPBS supplemented with Rhodamine-Phalloidin (1.3 µL/mL) to each
284 of them. After 30 min in the dark, the inserts were cut and placed on microscope slides with
285 one drop of Vectashield® mounting medium containing DAPI, staining cell nuclei in blue.
286 Data were analyzed by ZEN Blue software to obtain *x-y, y-z* and *x-z* images.

287 To quantify the amount of nanoparticles uptaken by Caco-2 cells, the flow cytometry
288 technique was used. The samples were prepared in a similar manner as for the transport
289 study. Thus, 500 µL of cell medium containing $5x10^5$ Caco-2 cells per well were seeded in a
290 24 well-plate. The cells were placed at 37°C overnight. After 3 washes with pre-warmed
291 HBSS, 500 µL of HBSS (control), NLC-HIP-DiD or SLN-HIP-DiD (particles concentration of

292 4 mg/mL) were added in each well. After 2 h of incubation at 37°C, cells were detached by
293 addition of 200 µL trypsin-EDTA per well. After 5 min, trypsin-EDTA activity was stopped by
294 adding 1 mL of DMEM. The samples were then centrifuged, the medium was aspirated and
295 replaced by 500 µL HBSS. The cells were analyzed using the BD FACSVerse™ flow cytometer
296 (BD Bioscience, USA). To visualize the cell viability, 1 µL of propidium iodide was added to
297 the samples before conducting the analysis. The FlowJo analysis software was used to treat
298 the data.

299

300 3.5. Nanoparticles behavior in transport medium

301 3.5.1. Particle size

302 To evaluate the stability of the nanoparticles dispersed in HBSS, the particle size distribution
303 was monitored during 2 h. Therefore, 300 µL of NLC-HIP-DiD or SLN-HIP-DiD were dispersed
304 in 30 mL HBSS at 37°C. The suspensions were placed in an incubator at 37°C under 80 rpm
305 agitation. Samples were withdrawn every hour and directly analyzed by DLS at 37°C on a
306 NICOMP™ 380 ZLS (PSS.NICOMP, Santa Barbara, CA, USA) using the dynamic viscosity of
307 water at 37°C (8.90×10^{-4} Pa.s). Data are expressed as mean diameter ± SEM.

308

309 3.5.2. Drug release

310 The drug release studies were conducted also in HBSS and were performed in the same
311 concentrations as for the transport study (11 µg/mL). The corresponding volume of
312 nanosuspensions was dispersed in HBSS pre-warmed at 37°C so as to have a global volume
313 (HBSS plus formulation) of 10 mL. Samples were placed in an incubator at 37°C with an
314 agitation of 80 rpm. Every 30 min, 300 µL aliquots were withdrawn from the vial and filtered
315 across 0.1 µm PVDF filters (Ultrafree®-MC VV, Merck Millipore) *via* centrifugation at 12 000 g
316 during 15 min at 4°C. The filtrates were immediately analyzed *via* HPLC according to the
317 method described above (2.2.1). The release studies were conducted for 2 h and sink
318 conditions were respected.

319

320 3.6. Statistical analysis

321 All the experiments were performed in triplicate and are presented as mean ± standard
322 error of mean (mean ± SEM). The normal distribution of the data was determined using a
323 Shapiro-Wilk statistic test. Analyses of variance (ANOVA) followed by Bonferroni's *post hoc*
324 test were conducted to compare EE, DL and cytotoxicity of the formulations. For other
325 analyses, the Mann-Whitney test was applied. The level of significance was set at
326 probabilities of *$p<0.05$, **$p<0.01$, and ***$p<0.001$ when compared with the control. Data
327 were treated and analyzed with the GraphPad Prism 8 program (CA, USA).

328

329 # 4. Results and discussion

330 ## 4.1. Nanoparticle characterization

331 LEU lipophilicity was modified by formation of a HIP by electrostatic interaction with sodium
332 docusate. The precipitation efficiency was 99.93 ± 0.02 (n=44), indicating that almost all LEU
333 was under a lipophilic complexed form.

334 The HIP was encapsulated in NLC and SLN formed by HPH following 5 homogenization cycles
335 at 500 bar. EE and D_L values are shown in Figure 1. No significant difference was observed
336 between NLC and SLN concerning the EE of LEU (84 ± 3% for NLC-HIP and 89 ± 2% for SLN-
337 HIP). Moreover, no significant difference in EE with original formulations was observed when
338 DiD was co-encapsulated with HIP (85 ± 1% for NLC-HIP-DiD and 85 ± 2% for SLN-HIP-DiD).
339 DiD being highly lipophilic (log P = 10.2, (Mérian et al., 2015)), was considered completely
340 encapsulated in the nanoparticles.

341

342 The nanoparticles were also characterized regarding their particle size and PDI which are
343 displayed in

344 Table 2. Both blank nanosuspensions presented a particle size around 115 nm. The loading
345 of HIP or HIP and DiD had no significant impact on particle size ($p>0.05$). The PDI of both
346 type of blank nanoparticles was around 0.2 and was not affected by the loading of the
347 complex alone or co-encapsulated with the fluorophore.

348

349 *Table 2: Particle size distribution of the solid lipid-based nanoparticles measured by DLS at 25 °C (results expressed as mean*
350 *± SEM, n=3, N=3)*

	Blank NLC	NLC-HIP	NLC-HIP-DiD	Blank SLN	SLN-HIP	SLN-HIP-DiD
Z-average (nm)	114 ± 14	104 ± 12	109 ± 7	115 ± 11	124 ± 5	122 ± 6
PDI	0.24 ± 0.07	0.18 ± 0.05	0.20 ± 0.02	0.19 ± 0.05	0.22 ± 0.01	0.23 ± 0.04

351

352 ## 4.2. Cell culture studies

353 ### 4.2.1. Cytotoxicity evaluation

354 The viability of Caco-2 and co-cultures of Caco-2 and HT29-MTX cells in presence of blank or
355 loaded nanoparticles was evaluated using the MTT assay. The same range of nanoparticle
356 concentrations, 0.5-18 mg/mL (i.e. 2.3-75.0 µg/mL of LEU for loaded nanoparticles), were
357 incubated with the cells. No impact on cell viability was observed upon SLN incubation
358 within this range of concentrations. Hence the IC_{50} for SLN cannot be calculated. The
359 measured IC_{50} values for blank and loaded NLC are presented in Figure 2. Regarding both cell
360 types, a slight but not significant increase of the IC_{50} was observed when loaded NLC were
361 incubated compared to blank nanoparticles (from 2.3 mg/mL to 3.2 mg/mL for Caco-2 and
362 from 4.1 mg/mL to 4.3 mg/mL for Caco-2/HT29-MTX). The IC_{50} measured with loaded
363 nanoparticles corresponded to a total LEU concentration of 14.8 µg/mL in the case of Caco-
364 2/HT29-MTX and 11.3 µg/mL when only Caco-2 cells were used. The ratio between the IC_{50}
365 values measured with Caco-2/HT29-MTX and Caco-2 is equivalent to the cell ratio used in
366 the wells, indicating that only Caco-2 viability was affected by the incubation with NLC. The
367 difference of behavior between NLC and SLN can be explained by the presence of C90 in
368 NLC. This oily compound is a water-insoluble surfactant that has already shown a slight
369 concentration-dependent cytotoxicity over Caco-2 cells, induced by the high content of
370 propylene glycol monoester (~90%) (Ujhelyi et al., 2012).

371

372 ### 4.2.2. Presence of mucus

373 The presence of mucus on Caco-2/HT29-MTX cell monolayers (mucin-secreting model) was
374 assessed by staining the cell monolayers at the surface of the inserts with Alcian Blue. The
375 positive charges induced by the basic isothiouronium groups of this dye were attracted by
376 the anionic sites of mucus. The images taken by microscope confirmed the homogeneous

377 presence of mucus on co-cultured monolayers. As it could be observed from Figure 3, Caco-2
378 monolayers (left) did not show any blue on the surface of the monolayers, whereas Caco-
379 2/HT29-MTX (right) exhibited a continued deep blue layer on the surface, confirming the
380 presence of mucus.

381 4.2.3. Intracellular uptake

382 The interaction of the nanocarriers with the cells was investigated qualitatively by confocal
383 microscopy and quantitatively by flow cytometry.

384 The confocal microscopy images, shown in Figure 4 (A), were taken on cell monolayers
385 incubated with DiD-loaded nanosuspensions for 2 h at 37°C, which were then fixed and
386 stained. The green channel corresponds to actin stained by Rhodamine-Phalloidin and the
387 red channel indicates the SLN-HIP-DiD and NLC-HIP-DiD. The images show the presence of
388 both type of nanoparticles inside the two cells monolayers, indicating the ability of the
389 nanocarriers to penetrate the enterocytes. Furthermore, both NLC and SLN nanoparticles
390 were able to cross the mucus layer present at the surface of the co-cultured cell monolayers.

391 The flow cytometry results conducted on Caco-2 cells are expressed in Figure 4 (B). The FACS
392 histograms show a clear difference between the Caco-2 cells being incubated with only HBSS
393 (APC-/A-) and the Caco-2 being co-incubated with the DiD-loaded SLN and NLC (APC-/A+).
394 The results confirmed quantitatively that both formulations were internalized by Caco-2 cells
395 with 82.0 % of the alive cells (PE-negative) indicating positive to DiD-loaded SLN and 98.8%
396 of the cells indicating positive to DiD-loaded NLC (APC-positive). The significant difference
397 (**, $p<0.01$) between the uptake of DiD-loaded SLN and DiD-loaded NLC could be explained
398 by the presence of C90, a monoester of caprylic acid. These compounds are known to
399 promote the intestinal absorption of active molecules in different ways: by enhancing the
400 paracellular transport, by inducing the transient opening of the tight junctions or by
401 facilitating the transcellular transport by fluidization of the cell membranes (Brayden et al.,
402 2014; Lindmark et al., 1995; Maher et al., 2018; Ukai et al., 2020).

403

404 4.2.4. *In vitro* evaluation of Leuprolide intestinal transport

405 The *in vitro* evaluation of the intestinal transport of LEU across the epithelial barrier was
406 conducted on Caco-2 cell monolayers (enterocyte-like model). The effect of mucus was
407 investigated using co-cultures of Caco-2 with HT29-MTX (mucin-secreting model). The
408 passage of LEU and LEU encapsulated in lipid nanoparticles under a lipidized form was
409 compared by quantification of the LEU content in the basolateral reservoir after incubation
410 of the formulations for 2 h on cell monolayers grown on inserts. TEER values were very
411 significantly decreased upon incubation with the formulations, Figure 5. The nanoparticles
412 were not responsible for this decrease as the same phenomenon was observed in the same
413 proportions with the controls, where only HBSS was incubated with the cells. Moreover, final
414 TEER values were still equivalent or above 200 $\Omega.cm^2$ which is considered an acceptable
415 value for this kind of experiments and superior to the *in vivo* values of the human intestinal
416 epithelium (12-69 $\Omega.cm^2$ (Béduneau et al., 2014)). The quantification of the transported LEU
417 enabled the calculation of the P_{app} (results are depicted in Figure 6). The data showed no
418 significant difference between the transport of free and encapsulated LEU across Caco-2 cell
419 monolayers, regardless of the formulations. Moreover, there were no statistical differences
420 between the P_{app} of free or encapsulated LEU across Caco-2 and across Caco-2/HT29-MTX
421 cell monolayers although the presence of the mucus barrier was assessed, see Figure 3.

422

423 The P_{app} values depicted in Figure 6, are weak and correspond to a transport of LEU below
424 0.3% of the incubated dose. Regarding the results corresponding to nanoparticle uptake,
425 showing that more than 80% of nanoparticles were internalized by Caco-2 cells (in the
426 conditions of the experiments), a higher LEU transportation rate across cell monolayers was
427 expected.

428 Actually, the results of interactions between formulations and cells obtained by CLSM and
429 flow cytometry testified the ability of the nanoparticles to cross the apical membrane of the
430 enterocytes. However, even if these results demonstrated high internalization, they did not
431 guarantee the capacity of SLN and NLC to cross the basolateral cell membrane. Indeed, by
432 measuring the fluorescence of the samples collected on the basolateral compartment of
433 Caco-2 cell monolayers, it was possible to estimate the passage of DiD-loaded SLN to be 1.8

434 % of the nanoparticles incubated with Caco-2 monolayers and 1.2% for Caco-2/HT29-MTX
435 co-cultured monolayers. In the case of NLC, the fluorescent measurements have shown that
436 less than 1% of the nanoparticles crossed the monolayers. These results suggested that the
437 higher internalization, and consequently the higher affinity, between NLC and enterocyte
438 cells was not necessarily a good indication of the transport of the nanoparticles across the
439 entire cell monolayer.

440 Furthermore, a potential explanation for the absence of difference in permeability between
441 free and encapsulated LEU could lie in a drug leakage from the nanoparticles before reaching
442 the monolayers. This would consequently limit the presumed advantages of peptide
443 encapsulation in the nanocarriers.

444

445 4.3. Nanoparticles behavior in transport medium

446 4.3.1. Particle size stability in HBSS

447 HBSS was used as transport media. The stability of nanoparticles was evaluated over 2 h in
448 this medium by monitoring particle size evolution using DLS, at 37°C. The results showed no
449 aggregation of NLC nor SLN. Indeed, the size of SLN was stable in HBSS with an initial mean
450 diameter of 145 ± 2 nm (PDI= 0.19 ± 0.01) and of 144 ± 2 nm (PDI= 0.19 ± 0.02) after 2 h at
451 37°C. These values were equivalent to the ones measured in water: 150 ± 2 nm (PDI= 0.2 ±
452 0.02) right after dispersion and of 147 ± 1 nm after 2 h in water at 37°C. Same observations
453 were made with NLC for which the initial mean diameter in HBSS was 127 ± 1 nm (PDI= 0.17
454 ± 0.01) and 126 ± 1 nm (PDI= 0.17 ± 0.02) after 2 hours at 37°C while, in water, it was
455 measured at 130 ± 1 nm (PDI= 0.18 ± 0.01) and 126 ±1 nm (PDI= 0.17 ± 0.01), respectively.

456

457 4.3.2. Drug release in transport medium

458 Concerning LEU release in HBSS, a burst release could be observed as soon as the
459 nanoparticles were dispersed in the medium, Figure 7. Indeed, within the first five min, 89%
460 LEU was released from NLC and 92% from SLN. However, there was no further release of the
461 peptide during the remaining 2 h. This important initial drug release can be attributed to the
462 platelet shape of solid lipid nanoparticles. Indeed, this particular structures present an

463 important surface to volume ratio. Consequently, the proportion of drug exposed at the
464 surface of the particles is higher than the drug in the core of the particles. Therefore the
465 exchanges between the drug and the surrounding medium are facilitated with potential
466 increase of drug leakage (Dumont et al., 2019a; Mehnert and Mäder, 2012). Furthermore,
467 the formation of HIP is based on an electrostatic interaction between the peptide and an
468 anionic surfactant. This electrostatic attraction can be modified by the surrounding medium.
469 Indeed, a recent study using Taylor Dispersion Analysis has shown that the release of LEU
470 from HIP-loaded SEDDS was favored with increasing ionic strength (Chamieh et al., 2019).
471 Then, in HBSS, with an ionic strength above 150 mM, it can be postulated that a majority of
472 the HIP was dissociated leading to a change in LEU lipophilicity and, consequently, let to a
473 higher extent of release from the solid lipid matrix of the nanoparticles. Furthermore, this
474 dissociation phenomenon sheds new light on the release profiles observed in FaSSIF-V2
475 (Dumont et al., 2019a). Indeed, LEU release from SLN and NLC observed in this medium was
476 originally assigned to the presence of phospholipids able to dissolve the peptide located at
477 the surface of the particles. However, as FaSSIF-V2 exhibits an ionic strength of 100 mM, this
478 parameter might be directly involved in the 65 to 70% of LEU released from the
479 nanocarriers. In addition, in the same study, the evaluation of nanoparticles stability in water
480 (0 mM) has shown almost no release of LEU in this neutral ionic strength environment over
481 several days (Dumont et al., 2019a). This would correlate Chamieh *et al.* observations with
482 peptide release increasing as a function of ionic strength.

483 Besides the alteration of HIP induced by ionic strength increase, the differences in pH of the
484 different media can also influence the stability of the complex. Indeed, the arginine (pKa=6)
485 and histidine (pKa=13) residues of LEU are positively charged under acidic conditions and
486 able to create electrostatic interactions with sodium docusate (pKa=-1°). However, when the
487 pH increases and gets closer to the pKa, the number of ionized functions decreases and the
488 interactions with the counterion become difficult to predict (Ristroph and Prud'homme,
489 2019). HBSS, FaSSIF-V2 and the aqueous suspensions of nanoparticles exhibit pH of 7.6, 6.8
490 and 5 respectively. Thus, in FaSSIF-V2 and water the difference pH-pKa is almost 1 unit with
491 consequently partial neutralization of the imidazole group of histidine, loss of complexation
492 with sodium docusate and consequently decrease in lipophilicity and affinity for the

493 nanocarrier. This effect may be even more pronounced in the case of HBSS with pH>pKa by
494 more than 1 unit.

495 The combination of pH and ionic strength differences might then explain the LEU release
496 observed in the different media.

497 The important drug release could explain the lack of differences between the transport free
498 LEU and encapsulated LEU across Caco-2 and Caco-2/HT29-MTX cell monolayers as the great
499 majority of the peptide could have left the particles before reaching the apical side of the
500 cells. Our hypothesis is that as the HIP is dissociated in the transport medium, both LEU and
501 the water-soluble anionic surfactant docusate are released. This latter compound can
502 fluidize enterocyte membrane if present under its Critical Micellar Concentration (2.37 mM
503 at 35°C, (Chakraborty et al., 2007)). In the present study, the maximal concentration of
504 docusate in the medium (if completely released from the nanoparticles) would be 1.78 10^{-5}
505 mM. However, as not improvement in peptide transport was observed, probable
506 interactions of docusate with the surrounding medium of high ionic strength should be
507 considered.

508 In view of the results, the stability of the lipidized peptide upon dispersion in biorelevant
509 media needs to be improved for the peptide to be retained inside the lipid nanocarriers. One
510 possibility would be to replace the docusate counterion. Indeed, Nazir *et al.* have recently
511 shown a LEU-pamoic acid HIP was relatively stable with a only 25% dissociation after 6 h in
512 phosphate buffer (pH=7.4, 154 mM NaCl) (Nazir et al., 2019a). The advantage of this
513 increased stability was verified during drug release studies in intestinal fluid (pH=6.8, 137
514 mM NaCl) where 60% of this HIP encapsulated in SEDDS remained in the lipophilic phase
515 after 4 h. Another option to retain hydrophilic peptides within lipid nanocarriers would be to
516 increase their hydrophobic character through H-bonds formation with non-ionic compounds
517 (Nazir et al., 2019b). As a matter of fact, this kind of interactions should be less sensitive to
518 the ionic strength and pH change of biorelevant media. Then, as the designed SLN and NLC
519 were able to cross the mucus barrier and were internalized by the enterocytes, the
520 encapsulation of stabilized lipidized peptide should increase their transport across the
521 intestinal barrier.

522

523 ## 5. Conclusion

524 In this study the lipophilicity of Leuprolide, a hydrophilic linear model peptide, was increased
525 by formation of a HIP with sodium docusate. The hydrophobic complex was loaded in SLN
526 and NLC obtained by HPH process with a high EE. Both particle types showed similar
527 physicochemical properties. The cytotoxicity of the nanoparticles in Caco-2 cells and co-
528 cultures of Caco-2 and HT29-MTX cells was evaluated. The results showed that only NLC
529 presented toxicity over the cells in the range of concentration tested. This toxicity was
530 attributed to the presence of propylene glycol monocaprylate (a liquid surfactant), which
531 probably interact more with cells than the solid esters comprising longer chain lengths.

532 The aim of the study was to evaluate *in vitro* the potential of the designed lipid nanoparticles
533 to cross the intestinal barrier and increase the transport of lipidized LEU. In this objective,
534 the interactions of the nanoparticles with Caco-2 cells (enterocyte-like model) and co-
535 cultures of Caco-2 and HT29-MTX cell lines (mucin-secreting model) were studied.

536 Images of the cell monolayers by CLSM after incubation of the formulation during 2 h in
537 HBSS have shown that both SLN and NLC were internalized by Caco-2 cells. Internalization
538 was also observed in the presence of mucus on Caco-2/HT29-MTX cell monolayers. Flow
539 cytometry measurements confirmed these observations with 82% SLN and 98.8% NLC being
540 internalized by Caco-2 cells. However, despite these promising results, the transport of LEU
541 across the cell monolayers was not improved by the encapsulation in lipid nanocarriers.
542 Indeed, most of the peptide was released in the transport medium probably due to the
543 platelet-shape of the lipid nanoparticles and a loss of lipophilicity of the peptide by
544 dissociation of the HIP in the transport medium. The increase in peptide lipophilicity should
545 be maintained in biorelevant media to benefit from the penetrating abilities of solid lipid
546 nanocarriers across the intestinal border.

547

548 ## 6. Acknowledgments

549 The present study was performed during the Short-Term Scientific Mission (STSM) between
550 Gattefossé/Lyon University and Louvain Drug Research Institute at the UCLouvain, and

551 received funding from COST Action 16205 UNGAP. A.B. is a research associate from the
552 Belgian F.R.S-FNRS (Fonds de la Recherche Scientifique).

553

554 ## 7. References

555 Almeida, A.J., Runge, S., Müller, R.H., 1997. Peptide-loaded solid lipid nanoparticles (SLN):
556 Influence of production parameters. International Journal of Pharmaceutics 149, 255–
557 265. https://doi.org/10.1016/S0378-5173(97)04885-0

558 Anderberg, E.K., Nyström, C., Artursson, P., 1992. Epithelial Transport of Drugs in Cell
559 Culture. VII: Effects of Pharmaceutical Surfactant Excipients and Bile Acids on
560 Transepithelial Permeability in Monolayers of Human Intestinal Epithelial (Caco-2) Cells.
561 Journal of Pharmaceutical Sciences 81, 879–887. https://doi.org/10.1002/jps.2600810908

562 Antoine, D., Pellequer, Y., Tempesta, C., Lorscheidt, S., Kettel, B., Tamaddon, L., Jannin, V.,
563 Demarne, F., Lamprecht, A., Béduneau, A., 2015. Biorelevant media resistant co-culture
564 model mimicking permeability of human intestine. International Journal of Pharmaceutics
565 481, 27–36. https://doi.org/10.1016/j.ijpharm.2015.01.028

566 Banerjee, A., Qi, J., Gogoi, R., Wong, J., Mitragotri, S., 2016. Role of Nanoparticle Size, Shape
567 and Surface Chemistry in Oral Drug Delivery. J Control Release 238, 176–185.
568 https://doi.org/10.1016/j.jconrel.2016.07.051

569 Béduneau, A., Tempesta, C., Fimbel, S., Pellequer, Y., Jannin, V., Demarne, F., Lamprecht, A.,
570 2014. A tunable Caco-2/HT29-MTX co-culture model mimicking variable permeabilities of
571 the human intestine obtained by an original seeding procedure. European Journal of
572 Pharmaceutics and Biopharmaceutics 87, 290–298.
573 https://doi.org/10.1016/j.ejpb.2014.03.017

574 Bonengel, S., Jelkmann, M., Abdulkarim, M., Gumbleton, M., Reinstadler, V., Oberacher, H.,
575 Prüfert, F., Bernkop-Schnürch, A., 2018. Impact of different hydrophobic ion pairs of
576 octreotide on its oral bioavailability in pigs. Journal of Controlled Release 273, 21–29.
577 https://doi.org/10.1016/j.jconrel.2018.01.012

578 Brayden, D.J., Gleeson, J., Walsh, E.G., 2014. A head-to-head multi-parametric high content
579 analysis of a series of medium chain fatty acid intestinal permeation enhancers in Caco-2
580 cells. European Journal of Pharmaceutics and Biopharmaceutics 88, 830–839.
581 https://doi.org/10.1016/j.ejpb.2014.10.008

582 Brayden, D.J., O'Mahony, D.J., 1998. Novel oral drug delivery gateways for biotechnology
583 products: polypeptides and vaccines. Pharmaceutical Science & Technology Today 1, 291–
584 299. https://doi.org/10.1016/S1461-5347(98)00075-3

585 Chakraborty, A., Subrata Chakraborty, Saha, S.K., 2007. Temperature Dependant
586 Micellization of AOT in Aqueous Medium: Effect of the Nature of Counterions. Journal of

587 Dispersion Science and Technology 28, 984–989.
588 https://doi.org/10.1080/01932690701463175

589 Chamieh, J., Domènech Tarrat, A., Doudou, C., Jannin, V., Demarne, F., Cottet, H., 2019.
590 Peptide release from SEDDS containing hydrophobic ion pair therapeutic peptides
591 measured by Taylor dispersion analysis. International Journal of Pharmaceutics 559, 228–
592 234. https://doi.org/10.1016/j.ijpharm.2019.01.039

593 Chen, X.-M., Elisia, I., Kitts, D.D., 2010. Defining conditions for the co-culture of Caco-2 and
594 HT29-MTX cells using Taguchi design. Journal of Pharmacological and Toxicological
595 Methods 61, 334–342. https://doi.org/10.1016/j.vascn.2010.02.004

596 Doshi Nishit, Mitragotri Samir, 2010. Needle-shaped polymeric particles induce transient
597 disruption of cell membranes. Journal of The Royal Society Interface 7, S403–S410.
598 https://doi.org/10.1098/rsif.2010.0134.focus

599 Dubray, O., Jannin, V., Demarne, F., Pellequer, Y., Lamprecht, A., Béduneau, A., 2016. In-vitro
600 investigation regarding the effects of Gelucire® 44/14 and Labrasol® ALF on the secretory
601 intestinal transport of P-gp substrates. International Journal of Pharmaceutics 515, 293–
602 299. https://doi.org/10.1016/j.ijpharm.2016.10.012

603 Dumont, C., Bourgeois, S., Fessi, H., Dugas, P.-Y., Jannin, V., 2019a. In-vitro evaluation of
604 solid lipid nanoparticles: Ability to encapsulate, release and ensure effective protection of
605 peptides in the gastrointestinal tract. International Journal of Pharmaceutics 565, 409–
606 418. https://doi.org/10.1016/j.ijpharm.2019.05.037

607 Dumont, C., Bourgeois, S., Fessi, H., Jannin, V., 2018. Lipid-based nanosuspensions for oral
608 delivery of peptides, a critical review. International Journal of Pharmaceutics 541, 117–
609 135. https://doi.org/10.1016/j.ijpharm.2018.02.038

610 Dumont, C., Jannin, V., Miolane, C., Lelong, Q., Valour, J.-P., Urbaniak, S., Fessi, H., Bourgeois,
611 S., 2019b. A proof-of-concept for developing oral lipidized peptide Nanostructured Lipid
612 Carrier formulations. Journal of Drug Delivery Science and Technology 101394.
613 https://doi.org/10.1016/j.jddst.2019.101394

614 Geszke-Moritz, M., Moritz, M., 2016. Solid lipid nanoparticles as attractive drug vehicles:
615 Composition, properties and therapeutic strategies. Materials Science and Engineering: C
616 68, 982–994. https://doi.org/10.1016/j.msec.2016.05.119

617 Griesser, J., Hetényi, G., Kadas, H., Demarne, F., Jannin, V., Bernkop-Schnürch, A., 2018. Self-
618 emulsifying peptide drug delivery systems: How to make them highly mucus permeating.
619 International Journal of Pharmaceutics 538, 159–166.
620 https://doi.org/10.1016/j.ijpharm.2018.01.018

621 Griesser, J., Hetényi, G., Moser, M., Demarne, F., Jannin, V., Bernkop-Schnürch, A., 2017.
622 Hydrophobic ion pairing: Key to highly payloaded self-emulsifying peptide drug delivery
623 systems. International Journal of Pharmaceutics 520, 267–274.
624 https://doi.org/10.1016/j.ijpharm.2017.02.019

625 Hetényi, G., Griesser, J., Moser, M., Demarne, F., Jannin, V., Bernkop-Schnürch, A., 2017.
626 Comparison of the protective effect of self-emulsifying peptide drug delivery systems
627 towards intestinal proteases and glutathione. International Journal of Pharmaceutics 523,
628 357–365. https://doi.org/10.1016/j.ijpharm.2017.03.027

629 Hintzen, F., Perera, G., Hauptstein, S., Müller, C., Laffleur, F., Bernkop-Schnürch, A., 2014. In
630 vivo evaluation of an oral self-microemulsifying drug delivery system (SMEDDS) for
631 leuprorelin. International Journal of Pharmaceutics 472, 20–26.
632 https://doi.org/10.1016/j.ijpharm.2014.05.047

633 Leonaviciute, G., Bernkop-Schnürch, A., 2015. Self-emulsifying drug delivery systems in oral
634 (poly)peptide drug delivery. Expert Opinion on Drug Delivery 12, 1703–1716.
635 https://doi.org/10.1517/17425247.2015.1068287

636 Lesuffleur, T., Porchet, N., Aubert, J.P., Swallow, D., Gum, J.R., Kim, Y.S., Real, F.X.,
637 Zweibaum, A., 1993. Differential expression of the human mucin genes MUC1 to MUC5 in
638 relation to growth and differentiation of different mucus-secreting HT-29 cell
639 subpopulations. J. Cell. Sci. 106 (Pt 3), 771–783.

640 Li, P., Nielsen, H.M., Müllertz, A., 2012. Oral delivery of peptides and proteins using lipid-
641 based drug delivery systems. Expert Opinion on Drug Delivery 9, 1289–1304.
642 https://doi.org/10.1517/17425247.2012.717068

643 Lindmark, T., Nikkilä, T., Artursson, P., 1995. Mechanisms of absorption enhancement by
644 medium chain fatty acids in intestinal epithelial Caco-2 cell monolayers. J Pharmacol Exp
645 Ther 275, 958–964.

646 Maher, S., Heade, J., McCartney, F., Waters, S., Bleiel, S.B., Brayden, D.J., 2018. Effects of
647 surfactant-based permeation enhancers on mannitol permeability, histology, and
648 electrogenic ion transport responses in excised rat colonic mucosae. International Journal
649 of Pharmaceutics 539, 11–22. https://doi.org/10.1016/j.ijpharm.2018.01.008

650 Mehnert, W., Mäder, K., 2012. Solid lipid nanoparticles. Advanced Drug Delivery Reviews,
651 Most cited papiers in the history of advanced drug delivery reviews: a tribute to the 25th
652 anniversary of the journal 64, 83–101. https://doi.org/10.1016/j.addr.2012.09.021

653 Mérian, J., Boisgard, R., Bayle, P.-A., Bardet, M., Tavitian, B., Texier, I., 2015. Comparative
654 biodistribution in mice of cyanine dyes loaded in lipid nanoparticles. Eur J Pharm
655 Biopharm 93, 1–10. https://doi.org/10.1016/j.ejpb.2015.03.019

656 Nazir, I., Asim, M.H., Dizdarević, A., Bernkop-Schnürch, A., 2019a. Self-emulsifying drug
657 delivery systems: Impact of stability of hydrophobic ion pairs on drug release.
658 International Journal of Pharmaceutics 561, 197–205.
659 https://doi.org/10.1016/j.ijpharm.2019.03.001

660 Nazir, I., Shahzadi, I., Jalil, A., Bernkop-Schnürch, A., 2019b. Hydrophobic H-bond pairing: A
661 novel approach to improve membrane permeability. International Journal of
662 Pharmaceutics 118863. https://doi.org/10.1016/j.ijpharm.2019.118863

663 Phan, T.N.Q., Shahzadi, I., Bernkop-Schnürch, A., 2019. Hydrophobic ion-pairs and lipid-
664 based nanocarrier systems: The perfect match for delivery of BCS class 3 drugs. Journal of
665 Controlled Release 304, 146–155. https://doi.org/10.1016/j.jconrel.2019.05.011

666 Ristroph, K., Prud'homme, R., 2019. Hydrophobic ion pairing: encapsulating small molecules,
667 peptides, and proteins into nanocarriers. Nanoscale Adv.
668 https://doi.org/10.1039/C9NA00308H

669 Sambuy, Y., Angelis, I.D., Ranaldi, G., Scarino, M.L., Stammati, A., Zucco, F., 2005. The Caco-2
670 cell line as a model of the intestinal barrier: influence of cell and culture-related factors
671 on Caco-2 cell functional characteristics. Cell Biol Toxicol 21, 1–26.
672 https://doi.org/10.1007/s10565-005-0085-6

673 Shrestha, N., Bouttefeux, O., Vanvarenberg, K., Lundquist, P., Cunarro, J., Tovar, S., Khodus,
674 G., Andersson, E., Keita, Å.V., Dieguez, C.G., Artursson, P., Préat, V., Beloqui, A., 2018. The
675 stimulation of GLP-1 secretion and delivery of GLP-1 agonists via nanostructured lipid
676 carriers. Nanoscale 10, 603–613. https://doi.org/10.1039/C7NR07736J

677 Ujhelyi, Z., Fenyvesi, F., Váradi, J., Fehér, P., Kiss, T., Veszelka, S., Deli, M., Vecsernyés, M.,
678 Bácskay, I., 2012. Evaluation of cytotoxicity of surfactants used in self-micro emulsifying
679 drug delivery systems and their effects on paracellular transport in Caco-2 cell monolayer.
680 European Journal of Pharmaceutical Sciences 47, 564–573.
681 https://doi.org/10.1016/j.ejps.2012.07.005

682 Ukai, H., Iwasa, K., Deguchi, T., Morishita, M., Katsumi, H., Yamamoto, A., 2020. Enhanced
683 Intestinal Absorption of Insulin by Capryol 90, a Novel Absorption Enhancer in Rats:
684 Implications in Oral Insulin Delivery. Pharmaceutics 12, 462.
685 https://doi.org/10.3390/pharmaceutics12050462

686

687 Figure 1: Encapsulation efficiency (A) and drug loading (B) of LEU in NLC-HIP, NLC-HIP-DiD,
688 SLN-HIP and SLN-HIP-DiD (Data shown as mean ± SEM, n=3)

689

690 Figure 2: IC50 values of blank and HIP-loaded NLC after 2 h incubation with Caco-2 and Caco-
691 2/HT29-MTX cells (data expressed as mean ± SEM, n=3).

692

693 Figure 3: Microscope images of Caco-2 (left) and Caco-2:HT29-MTX cell monolayers (right)
694 after 45 min incubation in Alcian blue (magnification x400, Scale bar = 1000 µm)

695

696 Figure 4: (A) CLSM images of SLN-HIP-DiD and NLC-HIP-DiD with Caco-2 and Caco-2/HT29-
697 MTX co-cultured cells monolayers after 2h incubation at 37°C (x25). Scale bar = 50 µm. The
698 green channel indicates Rhodamine-Phalloidin and the DiD-loaded nanoparticles are
699 indicated by the red channel. (B) Cellular uptake in Caco-2 cells of SLN-HIP-DiD (blue) and
700 NLC-HIP-DiD (orange) measured by flow cytometry, Caco-2 cells incubated with 500 µL of
701 HBSS are shown as controls. The table presents the percentage of APC positive (DiD-loaded
702 nanoparticles) among the PE negative (living cells) cells and the mean fluorescence intensity
703 of the APC channel (n=10, N=3, data expressed as mean ± SEM)

704

705 Figure 5: TEER values of Caco-2 (A) and Caco-2/HT29-MTX cell monolayers, before and after
706 incubation with formulations

707

708 Figure 6: P_{app} of neat and encapsulated LEU in SLN and NLC after 2 h incubation on Caco-2
709 and Caco-2/HT29-MTX cell monolayers (n=3, N=3, data expressed as mean± SEM)

710

711 Figure 7: In-vitro release profile of LEU from NLC-HIP-DiD and SLN-HIP-DiD in HBSS at 37°C
712 over 2 h (data expressed as mean ± SEM)

***Conflict of Interest**

Declaration of interests

☐ The authors declare that they have no known competing financial interests or personal relationships that could have appeared to influence the work reported in this paper.

☒The authors declare the following financial interests/personal relationships which may be considered as potential competing interests:

Camille Dumont, Cédric Miolane, and Vincent Jannin were employed by Gattefossé (Saint-Priest, France – *at the time of the study*), who manufactures Capryol® 90 and Precirol® ATO 5 used in this study.

***Credit Author Statement**

Solid lipid Nanocarriers diffuse effectively through mucus and enter intestinal cells – *but where is my peptide?*

Camille Dumont : Investigation ; Roles/Writing - original draft

Ana Beloqui : Conceptualization, Data curation; Supervision ; Writing - review & editing

Cédric Miolane : Investigation

Sandrine Bourgeois : Supervision

Véronique Préat : Conceptualization, Funding acquisition; Supervision

Hatem Fessi : Supervision

Vincent Jannin : Conceptualization, Funding acquisition; Supervision ; Writing - review & editing

Figure(s)

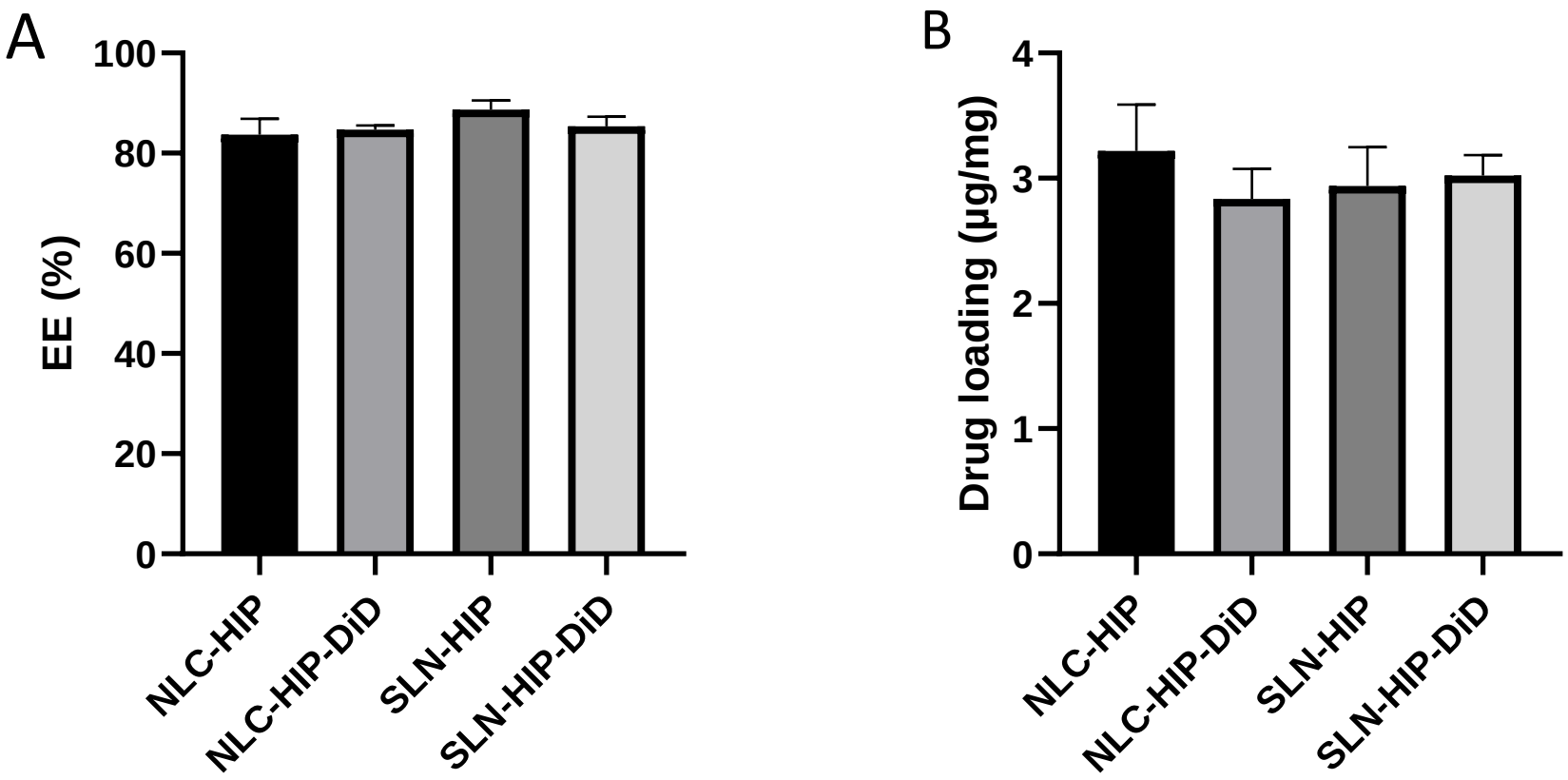
A
100
80
60
40
20
0
EE (%)
NLC-HIP
NLC-HIP-DiD
SLN-HIP
SLN-HIP-DiD
B
4
3
2
1
0
Drug loading (µg/mg)
NLC-HIP
NLC-HIP-DiD
SLN-HIP
SLN-HIP-DiD

Figure(s)

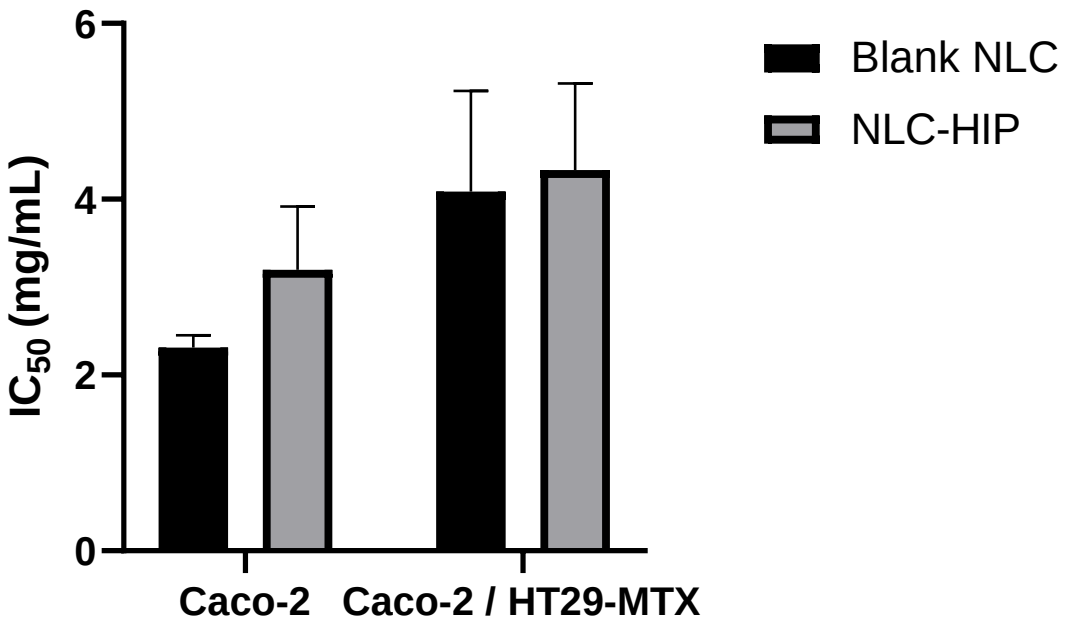

Figure(s)

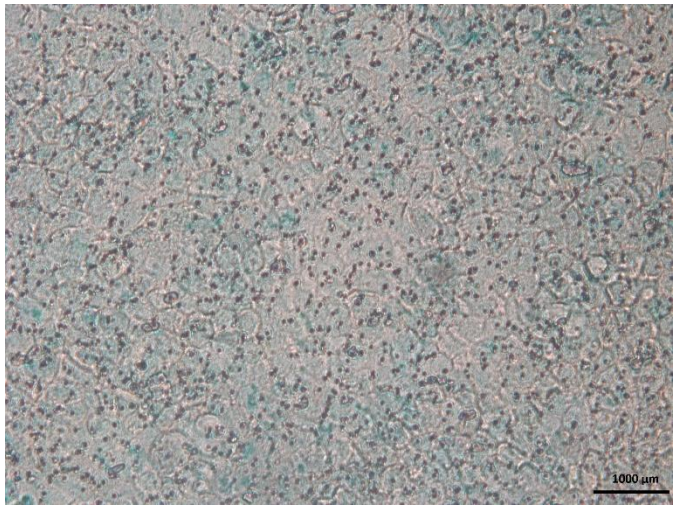

Caco-2

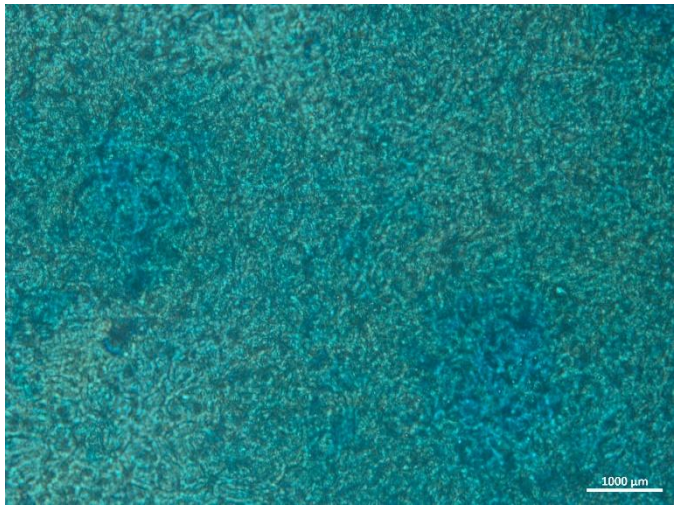

Caco-2:HT29-MTX (3:1)

Figure(s)

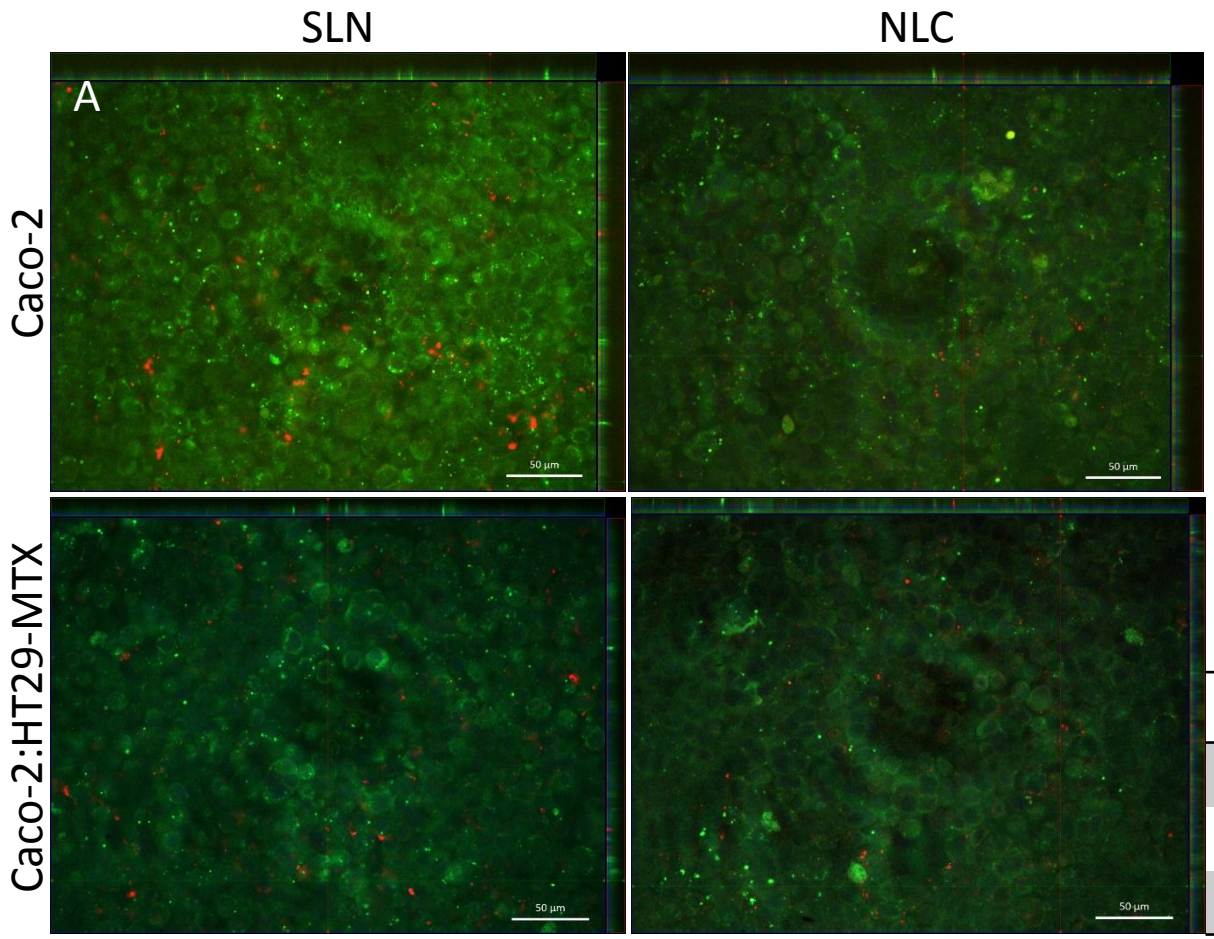

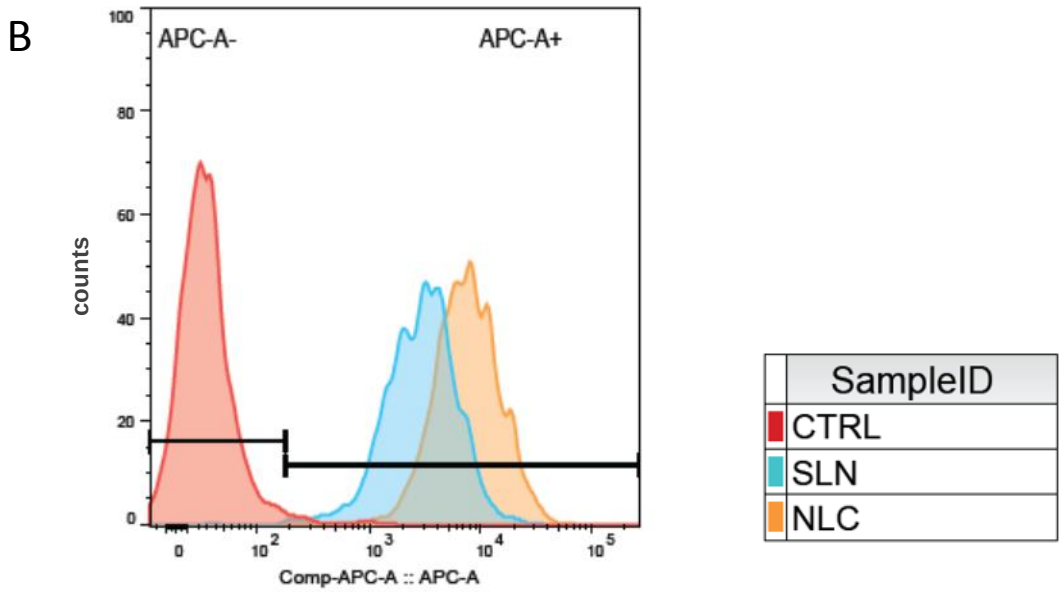

	% APC + /PE - cells	Mean Fluorescence intensity (a.u.)
Control	0.8 ± 0.1	32 ± 2
SLN	82.0 ± 4.6	1582 ± 438
NLC	98.8 ± 0.3	4558 ± 791

Figure(s)

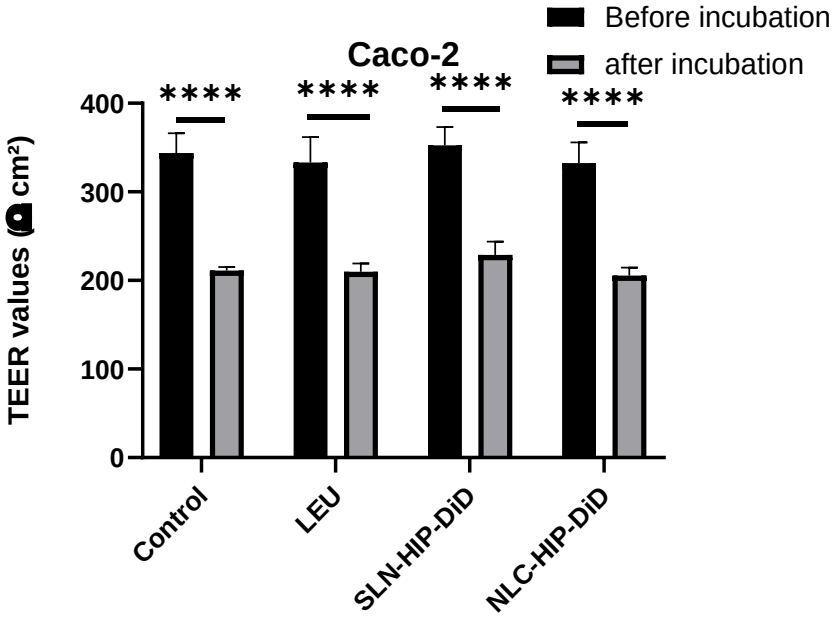
Caco-2
Before incubation
after incubation
TEER values (Ω cm²)
400
300
200
100
0
****
****
****
****
Control
LEU
SLN-HIP-DiD
NLC-HIP-DiD

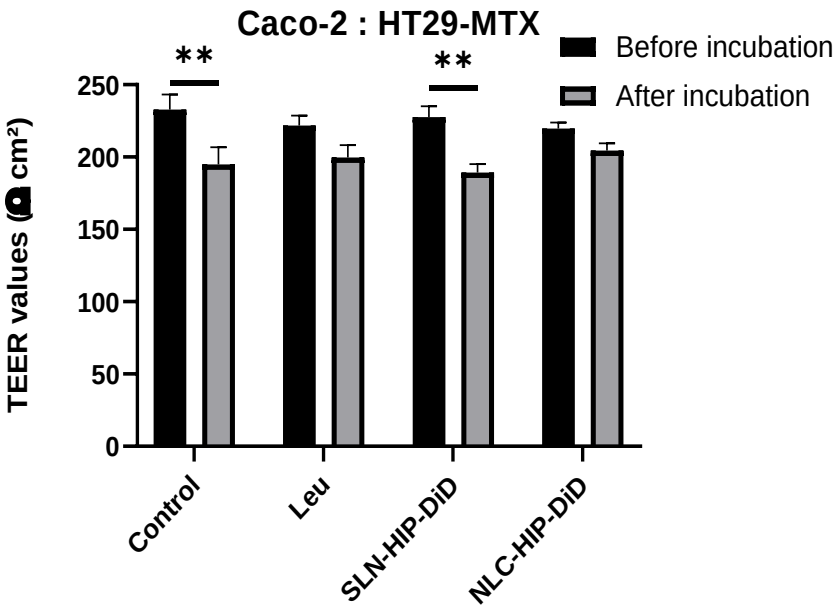
Caco-2 : HT29-MTX
Before incubation
After incubation
TEER values (Ω cm²)
250
200
150
100
50
0
**
**
Control
Leu
SLN-HIP-DiD
NLC-HIP-DiD

Figure(s)

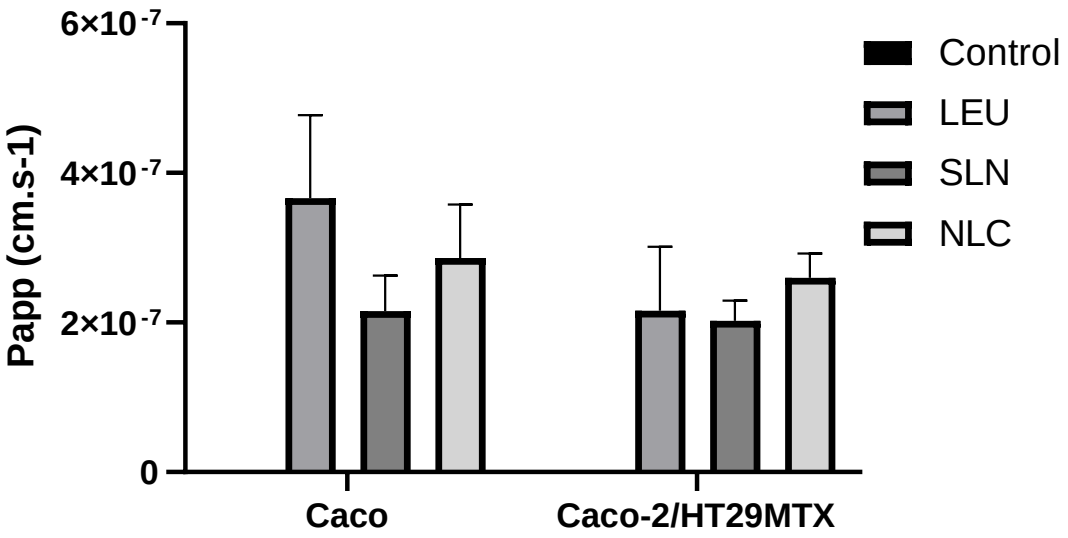
6×10-7
4×10-7
2×10-7
0
Papp (cm.s-1)
Caco
Caco-2/HT29MTX
Control
LEU
SLN
NLC

Figure(s)

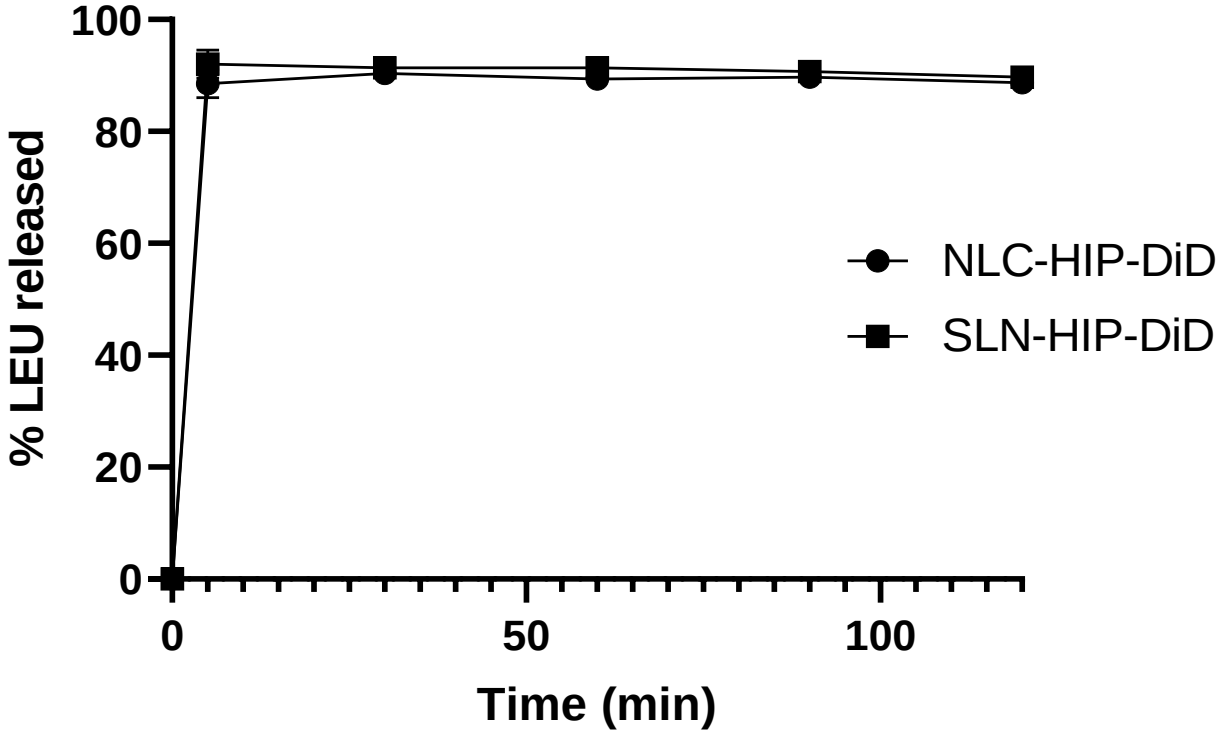
100
80
60
40
20
0
% LEU released
0
50
100
Time (min)
NLC-HIP-DiD
SLN-HIP-DiD